IOP Publishing Nanotechnology
Nanotechnology 29 (2018) 265103 (14pp) https://doi.org/10.1088/1361-6528/aabbd0

VSION as high field MRI T_1 contrast agent: evidence of their potential as positive contrast agent for magnetic resonance angiography

T Vangijzegem[1,3], D Stanicki[1], S Boutry[2], Q Paternoster[1], L Vander Elst[1], R N Muller[1,2] and S Laurent[1,2]

[1] Department of General, Organic and Biomedical Chemistry, NMR and Molecular Imaging Laboratory, University of Mons, B-7000 Mons, Belgium
[2] Center for Microscopy and Molecular Imaging, Rue Adrienne Bolland, 8, B-6041 Gosselies, Belgium

E-mail: thomas.vangijzegem@umons.ac.be

Received 10 January 2018, revised 28 March 2018
Accepted for publication 5 April 2018
Published 4 May 2018

Abstract

Because of their outstanding magnetic properties, iron oxide nanoparticles have already been the subject of numerous studies in the biomedical field, in particular as a negative contrast agent for T_2-weighted nuclear magnetic resonance imaging, or as therapeutic agents in hyperthermia experiments. Recent studies have shown that below a given particle size (i.e. 5 nm), iron oxide may be used to provide a significant positive (brightening) effect on T_1-weighted MRI. In such an application, not only the size of the crystal, but also the control of the coating process is essential to ensure optimal properties, especially at a very high field (> 3 T). In this work, we focused on the development of very small iron oxide nanoparticles as a potential platform for high field T_1 magnetic resonance angiography (MRA) applications. The feasibility has been evaluated *in vivo* at 9.4 T, demonstrating the usefulness of the developed system for MRA applications.

Supplementary material for this article is available online

Keywords: magnetic resonance imaging, iron oxide nanoparticles, T_1 contrast agents, magnetic resonance angiography, high field MRI

(Some figures may appear in colour only in the online journal)

Introduction

Magnetic resonance imaging (MRI) is probably one of the most powerful and useful medical diagnosis tools, enabling the exploration of the internal tissues without surgery [1]. The poor sensitivity of the technique can be drastically enhanced by the administration of exogenous contrast agents [2]. Such compounds, typically paramagnetic ions exhibiting a high number of unpaired electrons, speed up the proton relaxation, inducing a modification (an increase or a decrease) of the signal intensity in their accumulation zone. Gadolinium-based contrast agents (Gd complexes) are among the most used for (pre)clinical applications because of their brightening effect on the signal (the so-called T_1 effect) [3]. In most cases, these chelates are characterised by an early extravasation and a fast renal clearance [4], making them suitable, for example, for the detection of altered tissues. However, when longer scanning times are needed (for example, for the study of micro-vascularization or high-resolution imaging), such elimination kinetics is not compatible. Several attempts have been made to circumvent this limitation, such as plasma protein labelling (mainly albumin), or the use of high molecular weight ligands [5]. Other systems in which gadolinium atoms are embedded inside a nanoplatform have also been reported [6].

[3] Author to whom any correspondence should be addressed.

Although extensively used in clinical diagnosis, one must stress that gadolinium derivatives have several disadvantages, the worst being the toxicity of free Gd ions [7]. Moreover, besides the well-known nephrogenic systemic fibrosis affecting patients with severe kidney failure, recent reports have highlighted a dose-dependent gadolinium accumulation in the brain of healthy patients [8]. Such behaviour having been observed for patients treated with linear Gd complexes (i.e. DTPA) [9] underlines the need of a safe and efficient alternative [10]. One of these, already a widely studied alternative, is the use of superparamagnetic nanoparticles. Thanks to their strong magnetic moment, these nanosystems are known to induce local magnetic inhomogeneities leading to a remarkable transverse relaxivity increase, thus darkening strongly their area of accumulation [11]. Despite clinical use till the late 1990s, their success has been hampered by several disadvantages, such as the well-known "blooming effect" [12], or the intrinsic dark signal of T_2-weighted MRI which can be confusing during diagnosis establishment [13]. Interestingly, recent reports have shown that a brightening effect can be obtained for such compounds when decreasing the size of the particles below a critical value (i.e. 5 nm) [12–15]. Such behaviour for very small iron oxide nanoparticles (VSIONs) has been described as the consequence of the decrease of the net nanoparticles' magnetic moment due to the reduction in the magnetic anisotropy of the core, along with spin disorder on the surface of the nanoparticles [16, 17]. On the other hand, the particle area to volume ratio increases dramatically, inducing an increase in the number of surface paramagnetic ions and subsequently inducing local relaxation change in the nearby water protons, thus affecting T_1. When targeting these applications, the monodispersity of the sample has to be ensured. Many synthesis methods have been described to prepare such nanosystems [18]. However, the thermal decomposition of an iron complex (e.g. iron oleate, iron acetylacetonate) in high boiling apolar solvents (e.g. dibenzylether, oleyl alcohol) appears to be the most efficient process to produce well-defined (in size and shape) and highly crystalline nanoparticles [19, 20]. The major drawback of this method lies in the surface modification needed to transfer the particles in aqueous media [21, 22]. Indeed, the thermal decomposition proceeds in the presence of long chain surfactants, leading to the formation of hydrophobic systems [23–25]. However, one must stress that such modification can induce the formation of agglomerates, inducing inevitably a significant increase of the transverse relaxivity alongside a slight decrease of the longitudinal relaxivity [26, 27], thus limiting their T_1 effect.

In this study, we propose the preparation of a nanoplatform suitable for T_1-weighted magnetic resonance angiography (MRA). Although this kind of application has already been investigated, the authors typically focused their studies on clinical magnetic fields (i.e. 1.5 T or 3 T) [28]. Being aware that the longitudinal relaxivity evolves with the strength of the magnetic field (after 0.5 T, r_1 decreases when increasing the magnetic field), we were interested in whether this kind of application would be feasible at a higher field (> 3 T). To achieve that goal, care must be taken, firstly with the preparation of nanoplatforms smaller than 5 nm, with great control over the size and the size distribution, and secondly with the transfer of the as-prepared samples in aqueous media while avoiding the formation of agglomerates.

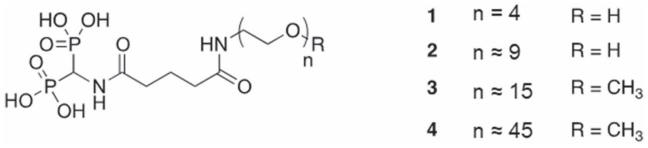

Figure 1. Chemical structures of the ligand used for very small iron oxide nanoparticle (VSION) stabilisation.

After the development of experimental conditions to obtain VSIONs by hot injection, aqueous transfer was optimised by means of the introduction of polyethyleneglycol (PEG)-based ligands (figure 1). After analysing the stability of the as-obtained platform, its efficiency as a potential platform for T_1-weighted MRA was attested using high field MRI (9.4 T).

Experimental section

Materials

Oleylamine (98%), oleic acid (90%), dibenzylether (99%), diphenylether (99%), hexadecane (99%), octadecene (90%), iron(III) acetylacetonate (99.9%), nitric acid, hydrogen peroxide, triethyl orthoformate (98%), diethyl phosphite (98%), dibenzylamine (97%), trimethylsilyl bromide (TMSBr; >97%), glutaric anhydride (95%), tetraethyleneglycol (99%), polyethyleneglycol (M_n 400), *O*-(2-aminoethyl)-*O*′-methylpolyethyleneglycol (750 g/mol), *O*-(2-aminoethyl)-*O*′-methylpolyethyleneglycol (2000 g/mol), p-toluenesulfonylchloride (⩾99%), sodium azide (⩾99.5%), diisopropylethylamine (⩾99%), diisopropylcarbodiimide (DIC; 99%), silver(I) oxide (⩾99.5%) and palladium on charcoal (10%) were purchased from Sigma-Aldrich (Belgium). Further, 1,2 hexadecanediol (98%), oleyl alcohol (>60%), octylether (>95%) and *N*-hydroxysuccinimide (NHS; >98%) were purchased from TCI Chemicals (Belgium). Dichloromethane (>99%), methanol (MeOH; 99.8%), ethanol (EtOH; 100%), diethylether (99.5%) tetrahydrofuran (THF; 99.9%), acetonitrile (ACN; 99%) and potassium iodide (99.5%) were purchased from Chemlab (Belgium). Resovist® was purchased from Schering (Germany). All the materials mentioned above were used without further purification. Membranes (MWCO = 30 000) for ultrafiltration were purchased from Millipore (USA).

Characterisation techniques

Transmission electron microscopy (TEM) was used to obtain detailed morphological information on the samples and was carried out using a Fei Tecnai 10 microscope operating at an accelerating voltage of 80 kV (Oregon, USA). The samples were prepared by placing a drop of diluted suspension of iron oxide nanoparticles on a carbon-coated copper grid (300 mesh; NP in organic media) or copper grid (300 mesh; NP in aqueous media), allowing the liquid to dry in air at room

temperature. The statistical treatment of the TEM images was performed by iTEM analysis (Münster, Germany) on multiple images for each sample. The mean diameter, the standard deviation and the polydispersity index (PDI) were calculated by measuring the particles' diameters. The number of nanoparticles counted ranged from 300–500.

The measurements of the size distribution and the zeta potential of the nanoparticles suspended in aqueous medium were performed on a Zetasizer nano zs (Malvern Instruments, United Kingdom) using a He-Ne laser (633 nm). The zeta potential was determined directly in a solution containing NaCl (0.01 mM). The pH of the aqueous suspension containing the particles was adjusted by adding 0.1–0.001 mM HNO_3 or NaOH solution.

Nuclear magnetic relaxation dispersion (NMRD) profiles were recorded on samples of iron oxide nanoparticles in physiological media (0,9% NaCl) with a field cycling relaxometer (Stelar, Mede, Italy) measuring the longitudinal relaxation rates (R_1) in a magnetic field range extending from 0.24 mT to 1 T. The temperature of the samples was adjusted to 37 °C with a precision of 0.1 °C. The theoretical adjustment of the NMRD profiles was performed with classical relaxation models [29, 30] assuming a diffusion coefficient of THF of 3.27 10^{-9} cm^2 s^{-1}. This diffusion coefficient was measured by diffusion-ordered NMR spectroscopy and was deduced from the average of three measurements for which diffusion coefficients were extracted and averaged from the two signals of THF appearing at 1.8 ppm and 3.6 ppm.

Longitudinal (R_1) and transverse (R_2) relaxation rate measurements at 0.47 T and 1.41 T were obtained on Minispec mq 20 and mq 60 spin analysers (Bruker, Germany) respectively. The relaxation rates were measured as a function of the iron molar concentration at 0.47 T and 1.41 T in order to calculate the r_1 and r_2 relaxivities (defined as the enhancement of the relaxation rate of water protons in 1 mmol/L solution of contrast agents). The relaxivities were calculated as the slope of the relaxation rate (R_i^{obs}) versus iron concentration according to the equation:

$$R_i^{obs} = \frac{1}{T_i^{obs}} = r_i[Fe] + \frac{1}{T_i^{dia}}$$

with r_i being the relaxivities and T_i^{dia} being the proton relaxation times of the solvent without nanoparticles.

The total iron concentration was determined by the measurement of the longitudinal relaxation rate R_1 according to the method previously described [31]. Briefly, the samples were mineralised by microwave digestion (MLS-1200 Mega, Milestone, Analis, Belgium) and the R_1 value of the resulting solutions was recorded at 0.47 T and 37 °C, which enabled the determination of the iron concentration using the equation:

$$[\mathrm{Fe}] = (R_1^{sample} - R_1^{dia}) \times 0.0915$$

where R_1^{dia} (s^{-1}) is the diamagnetic relaxation rate of acidified water (0.36 s^{-1}) and 0.0915 (s.mM) is the slope of the calibration curve.

^{1}H-NMR spectra were obtained using a Bruker Avance instrument (500 MHz), and chemical shifts (δ) are given in ppm, using TMS as an internal reference. The following abbreviations are used: *br* for broad, *s* for singlet, *d* for doublet, *t* for triplet, *q* for quadruplet, and *m* for multiplet.

IR spectra were recorded on a Perkin Elmer FTIR 1760K (Perkin Elmer, USA).

Mass spectra were recorded on a Q-TOF Ultima mass spectrometer (Water-Micromass, Manchester, UK).

Thermogravimetric analyses were carried out on a TA Instruments Q500 (New Castle, United States) using Pt crucibles. Prior to analysis, the samples were lyophilised and then washed with purified water to remove any contaminants. The resulting powder (10–30 mg) underwent first an isotherm of 10 min at 120 °C (heating rate: 10 °C min^{-1}) under nitrogen, followed by a heating ramp of 10 °C min^{-1} until reaching 600 °C under air. That temperature was maintained for a further 5 min.

Synthesis of very small iron oxide nanoparticle (VSION)

Typically, a mixture of oleic acid (2 mmol; 635 μl), oleylamine (2 mmol; 658 μl) and 1,2-hexadecanediol (10 mmol; 2.58 g) was solubilised in oleyl alcohol (10 ml) and heated at 300 °C for 10 min under nitrogen and magnetic stirring. Then a solution of iron (III) acetylacetonate (2 mmol; 706 mg) in oleyl alcohol (10 ml) was rapidly injected into the flask. The mixture was heated at 300 °C for a further 30 min, then rapidly cooled. The particles were isolated after pouring an excess of ethanol (40 ml) into the cooled solution, followed by magnetic decantation. Finally, the as-obtained precipitate was redispersed in tetrahydrofuran (10 ml) and centrifuged to remove any undissolved materials (16.000 g; 10 min).

Ligand preparation

*Synthesis of tetraethyl-N, N-dibenzyl aminomethyl-biphosphonate (**5**).* A mixture of triethylorthoformate (71 mmol; 10.6 g; 11.8 ml), diethyl phosphite (186 mmol; 25.6 g; 23.96 ml) and dibenzylamine (60 mmol; 11.81 g; 11.53 ml) was heated overnight at 150 °C under an argon atmosphere. The mixture was then treated with sodium hydroxide (5%) and the product extracted with dichloromethane. The organic layer was collected and the solvent was evaporated under reduced pressure. The oily residue was purified by liquid chromatography using hexane/ethyl acetate.

^{1}H-NMR (DMSO-d_6): δ (ppm): 7.3–7.2 (10H, m); 4.2–3.9 (12H, m); 3.3 (1H, t, $J_{P\text{-}H} = 24$ Hz); 1.2 (12H, t, $J = 7$ Hz).

MS (ESI-ToF) $C_{23}H_{35}NO_6P_2$ measured: m/z $(M + Na)^+$: 506.18.

*Synthesis of tetraethyl aminomethyl-biphosphonate (**6**).* A mixture of compound (**5**) (5.5 g) and palladium on carbon (Pd/C) (10%; 0.86 g) in ethanol (100 ml) was stirred under a hydrogen atmosphere and evaporated under reduced pressure to give a slightly yellowish oil.

^{1}H-NMR (DMSO-d_6): δ (ppm): 4.1 (8H, m); 3.6 (1H, t, $J_{P\text{-}H} = 21$ Hz); 1.3 (12H, t, $J = 7$ Hz).

MS (ESI-ToF) $C_9H_{23}NO_6P_2$ measured: m/z $(M + Na)^+$: 326.09.

*Synthesis of 5 -((bis (diethoxyphosphoryl) methylamino) -5-oxopentanoic acid (**7**).* A mixture of compound (**6**) (17 mmol; 4.78 g) and glutaric anhydride (25 mmol; 2.84 g) in acetonitrile (50 ml) was stirred for 24 h at room temperature. After this time, the solvent was evaporated under reduced pressure and the residue purified by liquid chromatography (dichloromethane/methanol mixture).

^{1}H-NMR (DMSO-d_6): δ (ppm): 12 (1H, s_{br}); 8.6 (1H, d, $J = 10$ Hz); 4.9 (1H, td, $J_{P\text{-}H} = 24$ Hz, $J_{H\text{-}H} = 10$ Hz); 4.1 (8H, m); 2.2 (4H, t, $J = 7$ Hz); 1.7 (2H, m, $J = 7$ Hz); 1.1 (12H, t, $J = 8$ Hz).

MS (ESI-ToF) $C_{14}H_{29}NO_9P_2$ measured: m/z $(M + Na)^+$: 440.12.

*Synthesis of succinimidyl 5-((bis (diethoxyphosphoryl) methylamino)-5-oxopentanoate (**9**).* A mixture of compound (**7**) (12 mmol; 5 g), *N*-hydrosuccinimide (180 mmol; 20.7 g) and *N*, *N*′-diisopropylcarbodiimide (120 mmol; 15.12 g) in dichloromethane (50 ml) was stirred for 24 h at room temperature under a nitrogen atmosphere. After this time, the mixture was filtered and the resulting filtrate collected before evaporation under reduced pressure. The residue was finally purified by liquid chromatography using a mixture of methanol/dichloromethane.

^{1}H-NMR ($CDCl_3$): δ (ppm): 6.76 (1H, d, $J = 10$ Hz); 5.01 (1H, td, $J_{P\text{-}H} = 22$ Hz, $J_{H\text{-}H} = 10$ Hz); 4.14 (8H, m); 2.82 (4H, s); 2.66 (2H, t, J = 7 Hz); 2.4 (2H, t, $J = 7$ Hz); 2.07 (2H, m, $J = 7$ Hz); 1.3 (12H, t, $J = 7$ Hz).

MS (ESI-ToF) $C_{18}H_{32}N_2O_{11}P_2$ measured: m/z $(M + Na)^+$: 537.14.

*Synthesis of α-tosyl-polyethyleneglycol 200 (**14**).* A mixture of tetraethyleneglycol (5.15 mmol; 1 g), silver (I) oxide (7.5 mmol; 1.79 g), para-toluenesulfonyl chloride (5.5 mmol; 1.08 g) and potassium iodide (1 mmol; 0.171 g) in dichloromethane (20 ml) was stirred for 24 h at room temperature. After discarding the catalyst, the filtrate was treated with water and extracted with dichloromethane. The organic solvent was dried over magnesium sulphate, then evaporated under reduced pressure to afford an oil which was finally purified by liquid chromatography using a dichloromethane/methanol mixture.

^{1}H-NMR ($CDCl_3$): δ (ppm): 7.77 (2H, d, $J = 7$ Hz); 7.32 (2H, d, $J = 7$ Hz); 4.14 (2H, t, $J = 5$ Hz); 3.55–3.70 (14H, m); 2.42 (3H, s).

*Synthesis of α-azide-polyethyleneglycol 200 (**16**).* A mixture of compound **14** (4.2 mmol; 1.47 g) and sodium azide (8.4 mmol; 0.55 g) in methanol (10 ml) was stirred for 24 h at 40 °C. After filtration and evaporation of the filtrate, the resulting oil was purified by chromatography using a dichloromethane/methanol mixture.

^{1}H-NMR ($CDCl_3$): δ (ppm): 3.64–3.74 (12H, m); 3.61 (2H, t, $J = 5$ Hz); 3.4 (2H, t, $J = 5$ Hz).

*Synthesis of α-amino-polyethyleneglycol 200 (**18**).* A mixture of compound **16** (0.6 mmol; 134 mg) and palladium-on-carbon (10%; 30 mg) in methanol (10 ml) was stirred under a hydrogen atmosphere at room temperature for 24 h. After discarding the catalyst by filtration, the resulting filtrate was evaporated under reduced pressure to obtain a yellow oil corresponding to the expected structure.

^{1}H-NMR ($CDCl_3$): δ (ppm): 3.64–3.74 (12H, m); 3.56 (2H, t, $J = 5$ Hz); 2.83 (2H, t, $J = 5$ Hz); 2.69 (2H, s_{br}).

*Synthesis of α-tosyl-polyethyleneglycol 400 (**15**).* A mixture of PEG 400 (10 mmol; 4 g), silver (I) oxide (15 mmol; 3.48 g), para-toluenesulfonyl chloride (10.5 mmol; 2 g) and potassium iodide (2 mmol; 0.32 g) in dichloromethane (40 ml) was stirred for 24 h at room temperature. After discarding the catalyst, the filtrate mixture was treated with water and extracted with dichloromethane. The organic solvent was dried over magnesium sulphate, then evaporated under reduced pressure to afford an oil which was finally then purified by liquid chromatography using a dichloromethane/methanol mixture.

^{1}H-NMR ($CDCl_3$): δ (ppm): 7.77 (2H, d, $J = 7$ Hz); 7.32 (2H, d, $J = 7$ Hz); 4.14 (2H, t, $J = 5$ Hz); 3.55–3.70 (34H, m); 2.42 (3H, s).

*Synthesis of α-azide-polyethyleneglycol 400 (**17**).* A mixture of compound **15** (10.5 mmol; 6 g) and sodium azide (21.6 mmol; 1.5 g) in methanol (25 ml) was stirred for 24 h at 40 °C. After filtration and evaporation of the filtrate, the resulting oil was purified by chromatography using a dichloromethane/methanol mixture.

^{1}H-NMR ($CDCl_3$): δ (ppm): 3.64–3.74 (32H, m); 3.61 (2H, t, $J = 5$ Hz); 3.42 (2H, t, $J = 5$ Hz).

*Synthesis of α-amino-polyethyleneglycol 400 (**19**).* A mixture of compound **17** (7.7; 3.4 g) and palladium-on-carbon (10%; 450 mg) in methanol (80 ml) was stirred under a hydrogen atmosphere at room temperature for 24 h. After discarding the catalyst by filtration, the resulting filtrate was evaporated under reduced pressure to obtain a yellow oil corresponding to the expected structure.

^{1}H-NMR ($CDCl_3$): δ (ppm): 3.64–3.74 (32H, m); 3.56 (2H, t, $J = 5$ Hz); 2.83 (2H, t, $J = 5$ Hz).

*Synthesis of compound **10**.* A mixture of α-amino PEG 200 **18** (2.97 mmol; 585 mg) and compound **9** (4.47 mmol; 2.3 g) in dichloromethane (5 ml) was stirred for 24 h at room temperature. After extraction, the aqueous phase was lyophilised and the resulting residue purified by liquid chromatography using a methanol/dichloromethane mixture.

^{1}H-NMR ($CDCl_3$): δ (ppm): 7.49 (1H, t, $J = 5$Hz); 7.14 (1H, d, $J = 10$ Hz); 5.1 (1H, td, $J_{P\text{-}H} = 22$ Hz, $J_{H\text{-}H} = 10$ Hz); 4.2 (8H, m); 3.6–3.8 (14H, m); 3.45 (2H, q, $J = 6$ Hz); 2.35 (2H, t, $J = 7$ Hz); 2.24 (2H, t, $J = 7$ Hz); 2.02 (2H, q, $J = 7$ Hz); 1.3 (12H, t, $J = 7$ Hz).

*Synthesis of compound **11**.* A mixture of α-amino PEG 400 **19** (1.25 mmol; 1 g) and compound **9** (1.9 mmol; 1 g) in dichloromethane (15 ml) was stirred for 24 h at room

temperature. After extraction, the aqueous phase was lyophilised and the resulting residue purified by liquid chromatography using a methanol/dichloromethane mixture.

^{1}H-NMR ($CDCl_3$): δ (ppm): 7.49 (1H, t, $J = 5$ Hz); 7.14 (1H, d, $J = 10$ Hz); 5.1 (1H, td, $J_{P\text{-}H} = 22$ Hz, $J_{H\text{-}H} = 10$ Hz); 4.2 (8H, m); 3.6–3.8 (36H, m); 3.45 (2H, q, $J = 6$ Hz); 2.35 (2H, t, $J = 7$ Hz); 2.24 (2H, t, $J = 7$ Hz); 2.02 (2H, q, $J = 7$ Hz); 1.3 (12H, t, $J = 7$ Hz).

Synthesis of compound ***12***. A mixture of methoxy (polyethyleneglycol)amine 750 (0.26 mmol; 200 mg) and compound **9** (0.3 mmol; 145 mg) in dichloromethane (10 ml) was stirred for 24 h at room temperature. After extraction, the aqueous phase was lyophilised and the resulting residue purified by liquid chromatography using a methanol/dichloromethane mixture.

^{1}H-NMR ($CDCl_3$): δ (ppm): 7.15 (1H, t, $J = 5$ Hz); 7.01 (1H, d, $J = 10$ Hz); 5.12 (1H, td, $J_{P\text{-}H} = 22$ Hz, $J_{H\text{-}H} = 10$ Hz); 4.19 (8H, m); 3.6–3.8 (65H, m); 3.45 (2H, q, $J = 5$ Hz); 2.30 (2H, t, $J = 7$ Hz); 2.21 (2H, t, $J = 7$ Hz); 1.99 (2H, q, $J = 7$ Hz); 1.32 (12H, t, $J = 7$ Hz).

Synthesis of compound ***13***. A mixture of α-amino PEG 2000 (0.26 mmol; 520 mg) and compound **9** (0.3 mmol; 145 mg) in dichloromethane (10 ml) was stirred for 24 h at room temperature. After extraction, the organic phase was dried over $MgSO_4$, the solvent evaporated under reduced pressure and the resulting residue purified by liquid chromatography using a methanol/dichloromethane mixture.

^{1}H-NMR ($CDCl_3$): δ (ppm): 7.15 (1H, t, $J = 7$ Hz); 7.01 (1H, d, $J = 10$ Hz); 5.12 (1H, td, $J_{P\text{-}H} = 22$ Hz, $J_{H\text{-}H} = 10$ Hz); 4.19 (8H, m); 3.6–3.8 (190H, m); 3.45 (2H, q, $J = 6$ Hz); 2.30 (2H, t, $J = 7$ Hz); 2.21 (2H, t, $J = 7$ Hz); 1.99 (2H, q, $J = 7$ Hz); 1.32 (12H, t, $J = 7$ Hz).

Synthesis of compound ***1***. A mixture of compound **10** (0.53 mmol; 315 mg) and trimethylsilylbromide (5.3 mmol; 700 μl) in dichloromethane (10 ml) was stirred for 24 h at room temperature under nitrogen. After evaporation of the solvent, the as-obtained residue was treated with methanol (10 ml) for 24 h at room temperature. After evaporation of the solvent, the product was extracted using a dichloromethane/water mixture, and recovered after lyophilisation of the aqueous phase.

^{1}H-NMR (D_2O): δ (ppm): 4.62 (1H, t, $J_{P\text{-}H} = 21$ Hz); 3.6–3.8 (14H, m); 3.3 (2H, t, $J = 7$ Hz); 2.29 (2H, t, $J = 7$ Hz); 2.21 (2H, t, $J = 7$ Hz); 1.82 (2H, q, $J = 7$ Hz).

Synthesis of compound ***2***. A mixture of compound **11** (0.1 mmol; 80 mg) and trimethylsilylbromide (1 mmol; 130 μl) in dichloromethane (10 ml) was stirred for 24 h at room temperature under nitrogen. After evaporation of the solvent, the as-obtained residue was treated with methanol (10 ml) for 24 h at room temperature. After evaporation of the solvent, the product was extracted using a dichloromethane/water mixture, and recovered after lyophilisation of the aqueous phase.

^{1}H-NMR (D_2O): δ (ppm): 4.36 (1H, t, $J_{P\text{-}H} = 21$ Hz); 3.6–3.8 (36H, m); 2.30 (4H, m); 1.89 (2H, q, $J = 7$ Hz).

Synthesis of compound ***3***. A mixture of compound **12** (0.1 mmol; 120 mg) and trimethylsilylbromide (1 mmol; 130 μl) in dichloromethane (10 ml) was stirred for 24 h at room temperature under nitrogen. After evaporation of the solvent, the as-obtained residue was treated with methanol (10 ml) for 24 h at room temperature. After evaporation of the solvent, the product was extracted using a dichloromethane/water mixture, and recovered after lyophilisation of the aqueous phase.

^{1}H-NMR (D_2O): δ (ppm): 4.36 (1H, t, $J_{P\text{-}H} = 21$ Hz); 3.6–3.8 (65H, m); 2.30 (4H, m); 1.89 (2H, q, $J = 7$ Hz).

Synthesis of compound ***4***. A mixture of compound **13** (0.1 mmol; 240 mg) and trimethylsilylbromide (1 mmol; 130 μl) in dichloromethane (10 ml) was stirred for 24 h at room temperature under nitrogen. After evaporation of the solvent, the as-obtained residue was treated with methanol (10 ml) for 24 h at room temperature. After evaporation of the solvent, the product was extracted using a dichloromethane/water mixture, and recovered after lyophilization of the aqueous phase.

^{1}H-NMR (D_2O): δ (ppm): 4.36 (1H, t, $J_{P\text{-}H} = 21$ Hz); 3.6–3.8 (189H, m); 2.30 (4H, m); 1.89 (2H, q, $J = 7$ Hz).

Synthesis of compound ***8***. A mixture of compound **7** (13 mmol; 5.42 g) and trimethylsilyl bromide (157 mmol; 20.75 ml) in dichloromethane (40 ml) was stirred for 24 h at room temperature under a nitrogen atmosphere. After evaporation of the solvent, the residue obtained was treated with methanol (20 ml) for 24 h at room temperature. After evaporation of the solvent under reduced pressure, the product was isolated by precipitation with an excess of acetonitrile.

^{1}H-NMR (D_2O): δ (ppm): 4.4 (1H, t, $J_{P\text{-}H} = 24$ Hz); 2.2 (4H, m); 1.7 (2H, q, $J = 7$ Hz).

Small animal imaging

A total of six mice were studied (n = 3 for each compound). CD1 female mice (6–11 weeks) were anaesthetised with isoflurane vaporised in oxygen and placed in a cradle adapted for mouse body imaging. Animal temperature was maintained by warm water circulating in a blanket during the whole anaesthesia period, and the respiratory rate was monitored in accordance with experimental protocol 2011-07 accepted by the ethics committee of CMMI (LA1500589). Mice were intravenously injected with VSIONs (45 micromoles Fe kg^{-1}) through a catheter (30 G needle) placed in a tail vein. MRI was performed with a Bruker Biospec 9.4 T scanner (Karlsruhe, Germany), using a 40 mm volume coil. Signal enhancement was dynamically observed on T1-weighted acquisitions with 1 min time resolution (FISP sequence: TR = 4.4 ms, TE = 1.5 ms, Flip Angle = 15°, NEX = 5,

resolution = 125 × 125 × 1000 micrometres). A series of 20 images was acquired and VSIONs were injected during the fifth image, allowing for a 16-min analysis. Another FISP image was acquired 1 h after injection. Signal enhancement in blood was measured by region of interest (ROI) drawing in the largest heart chamber seen on the image (ventricle) and expressed as a percentage relative to a mean signal intensity value calculated from the four pre-contrast acquisitions. Signal enhancement in the vena cava was illustrated using a RARE sequence (TR = 389.1 ms, TE = 8.1 ms, NEX = 6, resolution = 129 × 141 micrometres, slice thickness 1 mm). Signal darkening induced by VSION accumulation in liver was visualised by RARE sequence (TR = 2000 ms, TE = 17 ms, NEX = 5, resolution = 129 × 121 micrometres, slice thickness = 1 mm, RARE factor 4). Signal darkening was measured by ROI drawing in liver and was expressed as a percentage referring to the signal intensity collected on the pre-contrast image. Signal measurements were performed using Vivoquant software (Invicro, Boston, USA). Kidney elimination of VSION was monitored with a multi-slice-multi-echo (MSME) T2-weighted sequence (TR = 2000 ms, TE = 7.5–181 ms (24 echoes), NEX = 2, resolution = 344 × 352 micrometres, slice thickness = 1 mm). T2 was measured in renal pelvis using Paravision 5.1 software (Bruker, Karlsruhe, Germany).

Results and discussion

VSION synthesis and characterisation

The production of monodisperse nanoparticles is possible by separating nucleation and growth steps [32, 33]. This objective can be achieved by thermal decomposition. While most cases report the formation of VSION by heating [34–37], in our case, we decided to proceed by hot injection. Briefly, a solution of an organic iron complex solubilised in a high boiling temperature solvent is rapidly injected in a boiling solution of hydrophobic surfactants (e.g. oleic acid, oleylamine). The thermal shock undergone by the organometallic compound induces its decomposition and the formation of iron precursors (iron oxo-clusters), causing a supersaturation of the monomer concentration, which results in a very high nucleation rate. Then the formed nuclei can grow together to form nanoparticles [38]. In previous studies involving heating-up procedures, it has been demonstrated that the kinetics of the iron precursor decomposition, and consequently the final nanoparticle size, is greatly influenced by the nature of the solvent [39]. It thus seemed interesting to evaluate if such behaviour could also be observed in the case of hot injection. The standard protocol [38] involved the injection of iron (III) acetylacetonate (1 mmol) in a boiling solution of oleylamine, oleic acid and 1,2-hexadecanediol (1 mmol/1 mmol/5 mmol) for a reaction time of 30 min at 300 °C. The solvents used are summarised in table 1 (S.I.). Even if this is not the subject of the present paper, it seems important to note that the nature of the solvent has a great influence on the final nanoparticle size, the smallest being obtained in the presence of oleyl alcohol as a co-solvent, in agreement with other reports [39]. It should also be noted that upon injection, the temperature of the media falls to around 240 °C, then increases rapidly to stabilise at 300 °C. Consequently, the smaller mean size reached when working with oleyl alcohol suggests a higher stability of the iron complex (by the interaction of the terminal alcohol moiety with the iron complex), and a nucleation step at higher temperature, when compared with less polar solvents.

As a result, monodisperse nanoparticles with a mean diameter of 3.5 ± 0.6 nm (PDI: 1.11; figure S1 is available online at stacks.iop.org/NANO/29/265103/mmedia) have been obtained by using oleyl alcohol as solvent. Photocorrelation spectroscopy (figure S1) confirmed the formation of well-dispersed nano-structures characterised by a monomodal distribution and a small PDI of 0.090.

As already mentioned, one of the major drawbacks of the thermal decomposition method lies in the apolar nature of the resulting nanosystems. The transfer in aqueous media can be carried out after an additional step consisting either of the addition of amphiphilic ligands (e.g. polymers, alkylammonium salts or lipids) or in the exchange of the hydrophobic chain by hydrophilic ones [40]. The last procedure can imply the use of small charged molecules (citric acid or tetramethylammonium hydroxide) or the use of more sophisticated structures made of an oxide surface's anchoring moiety (e.g. dopamine, carboxylic acid, phosphonate or alkoxysilane) covalently attached to a stabilising group (polymer or ionisable functional group). This latter approach has been favoured in the context of this work. Thereby, we decided to prepare a ligand presenting on one side a strong anchoring group (bisphosphonate moiety), and on the other side, a PEG-based stabilising moiety (**1–4**; figure 1). The choice of phosphonate appeared obvious because of its strong interaction with iron oxide surfaces, as well as its property to form exclusively monolayers (in contrast to organosilane) [41–43]. In order to determine the optimum between stability and efficiency, four PEG chain lengths have been considered, varying from 4 to 45 monomer units.

Six steps were necessary to achieve the synthesis of these structures (figure 2), and involved first the preparation and the isolation of the activated succinimidyl ester **9** followed by its aminolysis after treatment with aminated PEG. For lower molecular sizes (i.e. PEG 200 and PEG 400), PEG was asymmetrically modified in three steps, including first silver (I) oxide/potassium iodide mediated monotosylation [44–46] followed by nucleophilic substitution with azide and concluded by pallado-catalysed hydrogenation to afford the targeted amino-PEG (figure 3). In a last step, successive treatments of compound **10–13** with trimethylsilylbromide (TMSBr) and methanol allowed the formation of phosphonic acid. A last structure (**8**; figure 2) presenting a carboxylic function was easily obtained by treating the acid **7** with TMSBr and methanol successively [47].

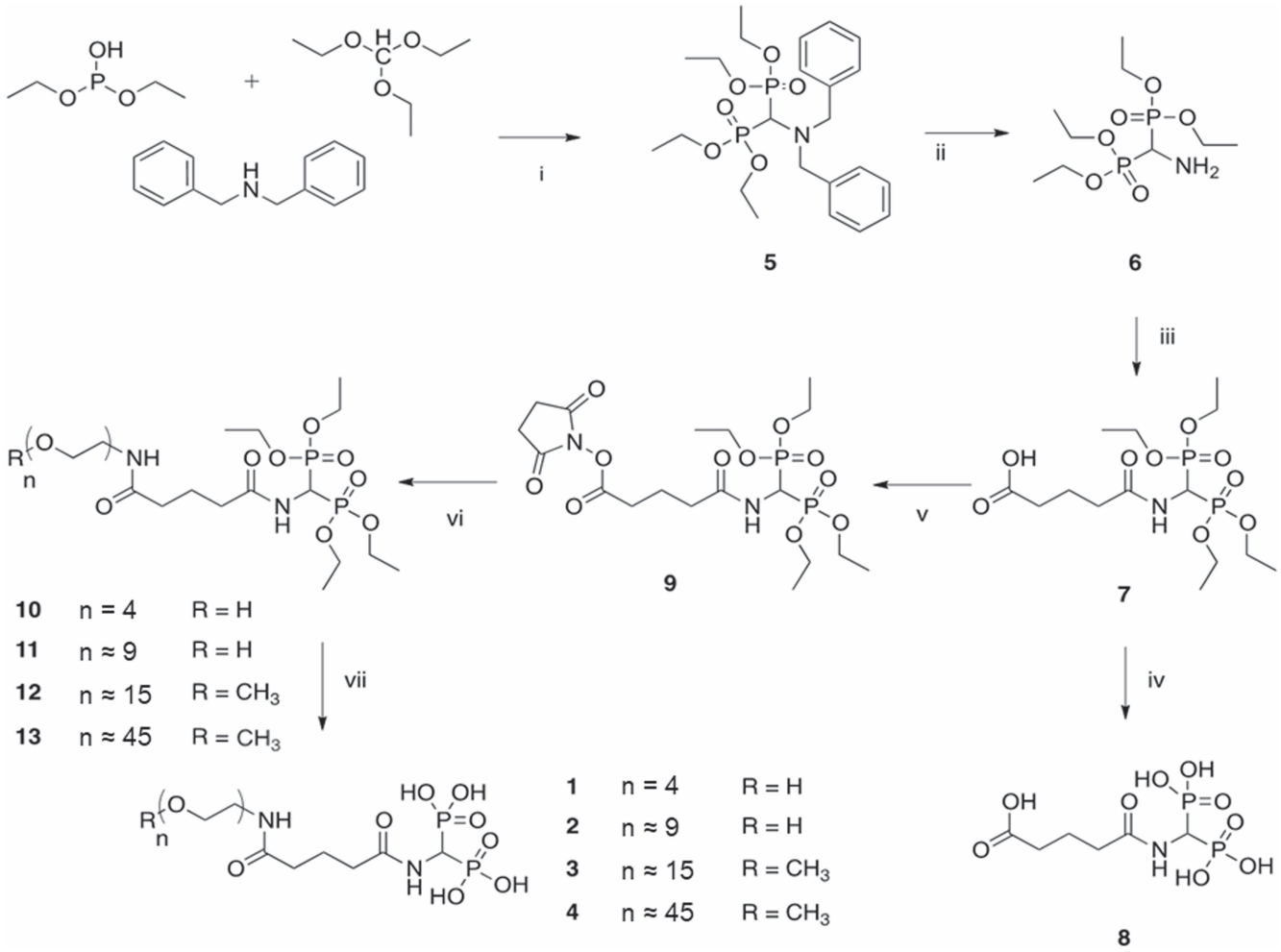

Figure 2. General procedure for the synthesis of ligands **1–4** and **8**. (i) Solvent-free, under refluxing conditions. (ii) EtOH saturated with dihydrogen, Pd/C (10%), 24 h r.t. (iii) Dichloromethane, succinic anhydride, 5 h r.t. (iv) Dichloromethane, TMSBr, 24 h r.t., then MeOH, 24 h r.t. (v) ACN, NHS/DIC, 10 h r.t. (vi) Dichloromethane, amino-PEG, 10 h r.t. (vii) Dichloromethane, TMSBr, 24 h r.t., then MeOH, 24 h r.t.

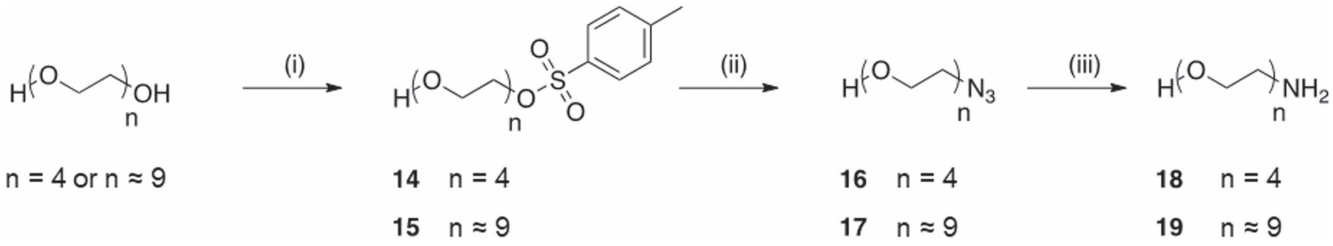

Figure 3. General procedure for the asymmetrical modification of PEG (**18**–**19**). (i) Dichloromethane, Ag_2O/KI, p-toluenesulfonyl chloride, 10 h r.t. (ii) MeOH, sodium azide, 60 °C, 10 h. (iii) EtOH saturated with dihydrogen, Pd/C (10%), 24 h r.t.

Transfer of the nanoparticles in aqueous media and characterisation

After conversion into phosphonic acid, the purified ligands were used to proceed to exchange experiments. A major difficulty that may occur in the context of nanoparticle transfer is the formation of aggregates. In the context of the magnetic resonance imaging, aggregate formation causes a significant increase in transverse relaxivity [29], limiting their use as T_1 agents. Using ligand **8** as a model system, different experimental conditions have been tested, including the solvent mixture, the pH and the concentration (table 2; S.I.). It appeared that the most efficient transfer took place in a tetrahydrofuran/water mixture (1/1), at pH 2.7 and with at least 1.25 mmol of ligand per mmol of elemental iron.

The comparison between VSION FTIR spectra before and after treatment with ligand **8** (figure 4(A)) suggests an efficient exchange process. Among the significant changes,

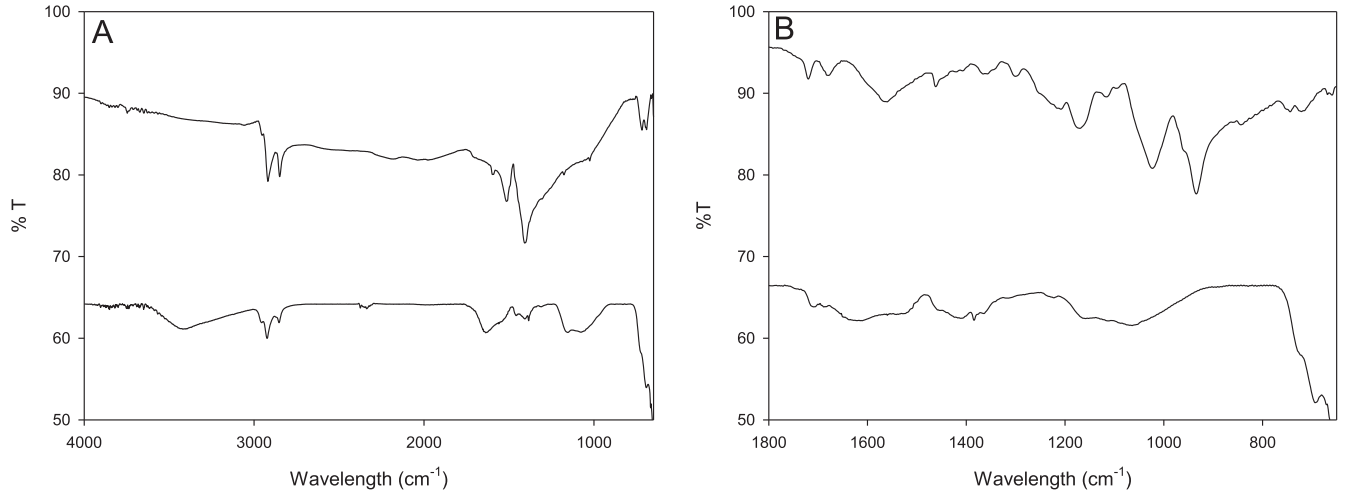

Figure 4. Comparison of FTIR spectra: (A) between VSION before (above) and after (below) ligand exchange, and; (B) between ligand **8** (above) and ligand **8**-treated VSION (below).

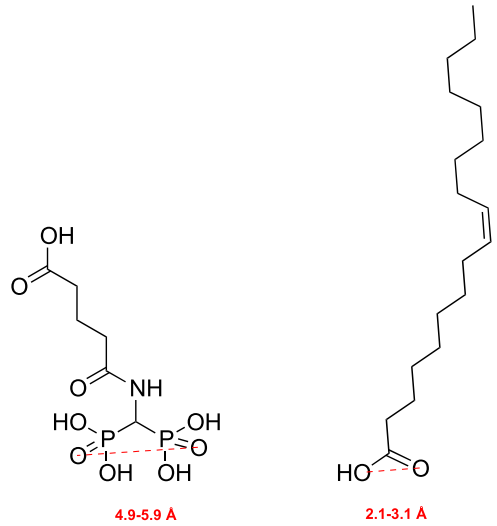

Figure 5. Illustration of the inter-atomic distances between oxygen atoms of phosphonic acid and those of oleic acid.

we can notice the appearance of a band at around 1720 cm^{-1} characteristic of carboxylic acid functions, along with the disappearance of the intense band at around 1400 cm^{-1} characteristic of the initial hydrophobic layer interacting with the surface of the iron oxide [48, 49]. When comparing the spectra of ligand **8** and VSION after exchange (figure 4(B)), especially the region between 1200 cm^{-1} and 800 cm^{-1}, we can observe the disappearance of the bands at around 1180 cm^{-1} (P = O) and 1038 and 940 cm^{-1} (P-OH), as well as the appearance of a fairly large band extending from 1200 to 950 cm^{-1}, which can be attributed to P-O-Fe vibrations.

The evolution of the zeta potential value *versus* the pH (figure S2) confirms the expected result by showing an isoelectric point at a pH value around 3.5, which is in accordance with the presence of the carboxylic functions onto the surface.

The number of ligand molecules (n_{ligand}) per nanoparticle has been estimated by thermogravimetric analysis using the following formula [50]:

$$\frac{organic\ wt\ \%}{inorganic\ wt\ \%} = \frac{n_{ligand}\ .M_w^{ligand}}{M_w^{VSION}}$$

where the molecular weight of the VSION (M_w^{VSION}) has been estimated from:

$$M_W^{VSION} = \rho\ .\ N_A.\ \frac{4}{3}\ .\ \pi\ .\ r_{VSION}^3$$

where N_A is the Avogadro number, ρ the maghemite density (5180 kg/m^3) and r the VSION radius (1.75 nm estimated by TEM).

Henceforth, assuming a total exchange, a surface density of around 1.8/nm^2 for ligand **8**-modified VSION has been deduced. When comparing this result to the surface density before exchange (assuming that the surface is fully covered by oleic acid species), which was estimated as around 2.9/nm^2, we can notice a significant decrease of the surface covering after exchange. This result could be explained by considering the inter-atomic distances of the functions assumed to interact with the surface of the particle. Whereas in the case of oleic acid, a distance of 2–3 Å between the two oxygen atoms is observed (figure 5), a distance of 5–6 Å can be observed between the oxygen atoms of the two phosphonic acids groups. However, these calculations should be considered with caution since they do not take into account steric effects and chain solvation.

A similar procedure was applied using PEGylated ligands (**1–4**). Interestingly, it is important to note that only the samples treated with ligands **3** (PEG750-VSION) and **4** (PEG2000-VSION) could be redispersed in an aqueous medium. For samples treated with ligands **1** (PEG-200) and **2** (PEG-400), no nanoparticle transfer was observed. The analyses carried out by infrared spectroscopy on ligand **2**-modified VSION (PEG400) (figure S3) show significant changes when compared to hydrophobic nanosystems; among them,

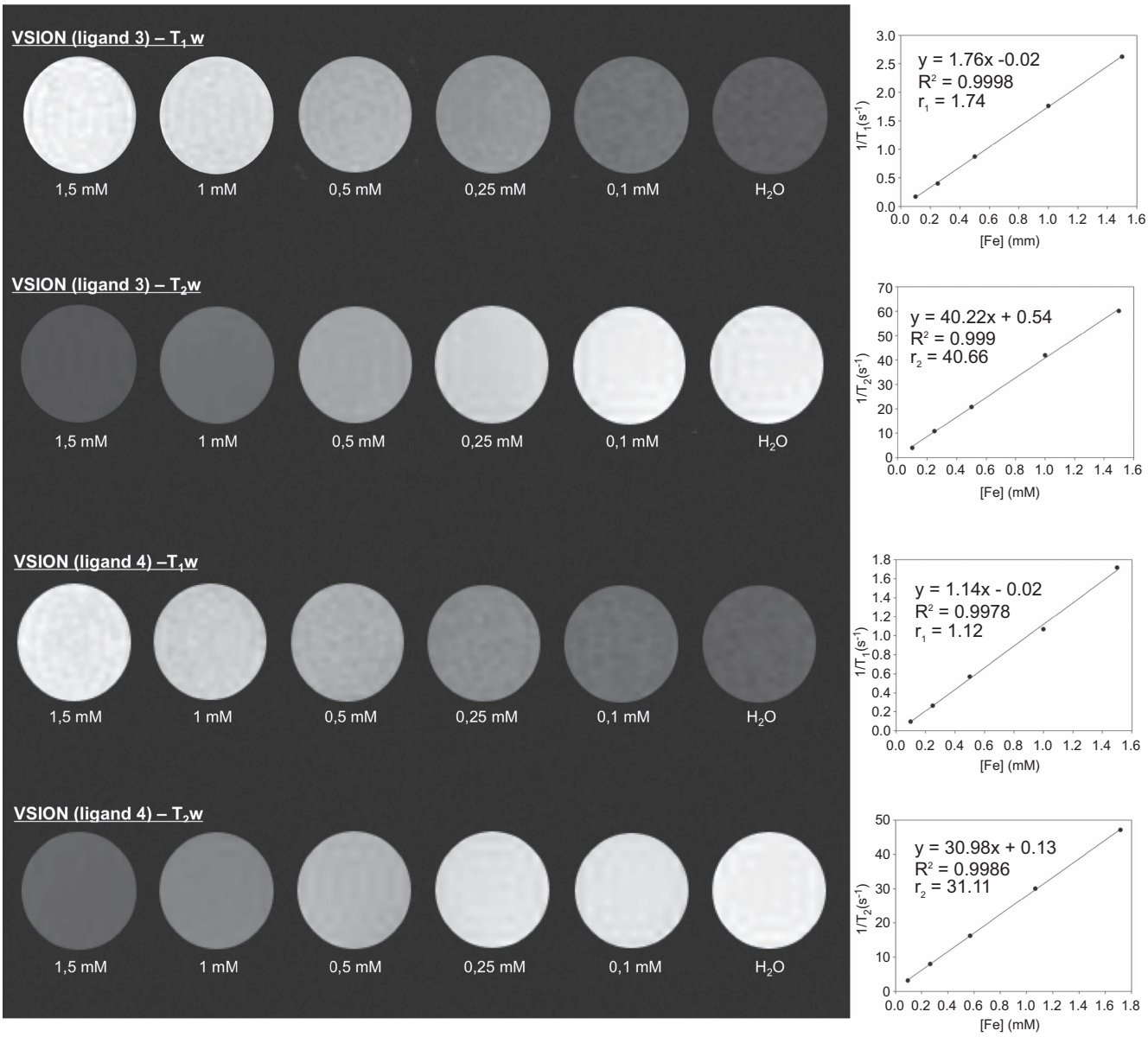

Figure 6. (left) Phantom MR images showing a concentration-dependent effect using T_1 and T_2 sequences (9.4 T); (right) plot of the relaxation rates *vs* the iron concentration for PEG750-VSION (above) and PEG2000-VSION (below).

the presence of a band at around 1660 cm^{-1} attributable to amide functions as well as bands extending from 900 to 1225 cm^{-1} attributable to the P-O-Fe vibrations. Moreover, important similarities between all the VSION FTIR spectra after exchange have been observed, confirming the presence of the PEGylated ligand on the surface (figure S3). These results could appear as surprising when taking into account that the smallest ligands, i.e. ligands **1–2**, exhibit similar or even higher sizes than oleic acid. The hypothesis chosen to explain this lack of stability in aqueous medium would be the spatial configuration of the ligand in solution, which would limit the interparticle steric repulsions. It can therefore be stated that a chain length of approximately 15 monomer units is required in order to transfer and stabilise nanoparticles of this size and composition in an aqueous medium.

In both cases, PEG-modified VSIONs exhibit a quite narrow monomodal size distribution in DLS (figure S4) with a mean diameter around 19.8 nm for PEG750-VSION and 22.2 nm for PEG2000-VSION. It should be noted that the mean diameter determined by TEM (figure S5) did not change after exchange, suggesting that no particle degradation occurred during the transfer process, as already reported in other studies using catechols [51].

Concerning the relaxivity values (table 3; S.I.), we notice a very slight increase of the r_2/r_1 ratio after the transfer step, suggesting that a slight agglomeration occurred during the exchange. However, one must stress that this increase is small compared to the high ratio values observed for agglomerating samples (up to several tens or even hundreds $s^{-1}mM^{-1}$) [52]. It should be noted that the ratio values were constant over a

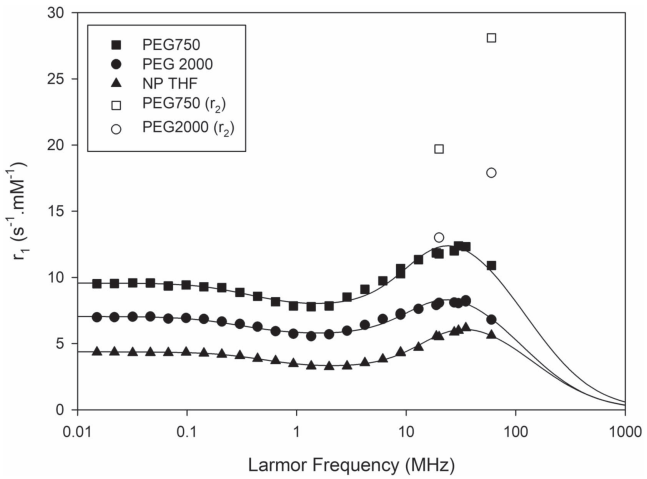

Figure 7. Nuclear magnetic relaxation dispersion (NMRD) profiles recorded for VSION before exchange (filled triangles) (solvent: THF), PEG750-VSION (filled squares) (solvent: H_2O), and PEG2000-VSION (filled circles) (solvent: H_2O); r_2 values at 20 MHz and 60 MHz for PEG750-VSION (empty squares) and PEG2000-VSION (empty circles).

period of three months, demonstrating the stability of the resulting platforms. When comparing the relaxivity values of our samples with the commercial agent Resovist® at 1.5 T, the PEG-modified VSIONs show similar longitudinal relaxivity but much lower r_2/r_1 ratios. Despite the large size of the resulting ligands (compared to oleic acid), especially for PEG2000, it appeared that longitudinal and transverse relaxivity values significantly increased after transfer for both VSION samples. That behaviour may result from the significantly lower ligand density obtained for both samples (i.e. 0.5 nm^{-2} for PEG750-VSION and 0.3 nm^{-2} for PEG2000-VSION) when compared to hydrophobic VSION (i.e. 2.9 nm^{-2}). This reduction in the number of ligands per unit area should facilitate the approach of the solvent molecule nearby the magnetic core doping, and thus the relaxivity. Finally, a decrease of nearly 60% in relaxivity values when increasing the PEG molecular weight was observed. Again, the ease of approach of the solvent molecule to the magnetic core will influence directly the relaxivities.

Given the low r_2/r_1, MR images of PEG2000-VSION and PEG750-VSION have been recorded using a 9.4 T scanner (400 MHz; figure 6). Considering the recorded NMRD profiles (figure 7), it clearly appears that the efficiency of VSION is lower at a high field, in agreement with the theoretical fitting using the standard relaxation model described for iron oxide nanoparticles [53]. With both PEG750-VSION and PEG2000-VSION, the obtained images (TR = 311 ms and TE = 8 ms) show a significant enhancement of the signal intensity in the presence of the particles, confirming the high potential of our platform as a T_1 agent. The comparison between MR images recorded for PEG750-VSION and Resovist® (figure S6) shows that the signal enhancement on T_1-weighted MRI is observed only for our platform. The demonstration of the T_1 effect observed at 400 MHz indicates the high stability of the presented systems.

As expected, a strong T_2 effect has also been highlighted (TR = 5000 ms and TE = 30 ms).

In vivo evaluation of PEG750-VSION and PEG2000-VSION

Both types of VSION-induced signal increase on dynamic acquisitions after i.v. injection, allowing for blood compartment signal enhancement as a positive contrast (figures 8(A); S7(A)). Signal increase was up to approximately 100% and remained at least at 80% enhancement during the whole dynamic acquisition (16 min), with no significant difference between compounds. However, the slope calculated from post-injection timepoints suggested that blood signal decreased more rapidly for PEG750-VSION ($-1.20 +/-0.31\%$ min^{-1}) than for PEG2000-VSION ($-0.47 +/-0.33\%$ min^{-1}; $p < 0.05$) (figure 9(A)). At this stage, it is difficult to correlate this behaviour to the respective VSION's properties. Perhaps smaller PEG chains of PEG750-VSION may give them a tendency toward a steeper blood concentration decrease because of a possible lower stealthiness regarding VSION-2000 that bears longer PEG chains. This result may correlate with the observation made by Weller and co-workers who showed that, depending on the size of the PEG grafted onto 4 nm particles, significant differences upon phagocytosis experiments were obsev nanoparticles with longer PEG chainred [54]. One must however stress that some of the studied samples showed poor stability in the culture, influencing their capture [54]. Another hypothesis may arise from their different hydrodynamic sizes, which may influence their clearance [55].

During this early circulation period, an interesting difference in terms of liver darkening related to VSION accumulation in mononuclear phagocyte system organs was observed (figures 8(C); S7(C)), 35 min after injection. The T_2 effect of PEG750-VSION induced a significantly greater liver signal decrease than PEG2000-VSION (-61% vs -44%; figure 9(B)). This probably reflects the combined influence of a stronger contrast effect of PEG750-VSION compared to PEG2000-VSION, and of slower liver uptake that may be expected from PEG2000-VSION (due to the reduced absorption of opsonins on nanoparticles with longer PEG chains [55]) regarding PEG750-VSION. This difference was no longer significant at 90 min post-injection (around -60% for both VSIONs). Image acquisition with dynamic sequence (FISP) one hour after injection revealed that the signal decrease was still approximately 60% higher as compared to the pre-contrast situation, suggesting progressive blood clearance of VSION. At day 1, enhancement was no longer visible and liver signal had decreased by another 10%.

T_2-weighted MRI using a multi-echo sequence allowed the showing of renal elimination of both types of VSION. Darkening was visible in renal pelvis at different times after i.v. injection of VSION (figures 8(D); S7(D)). This area recovered a clear aspect at day 1, looking similar to the pre-injection situation. The multi-echo approach allowed for T_2 measurement in

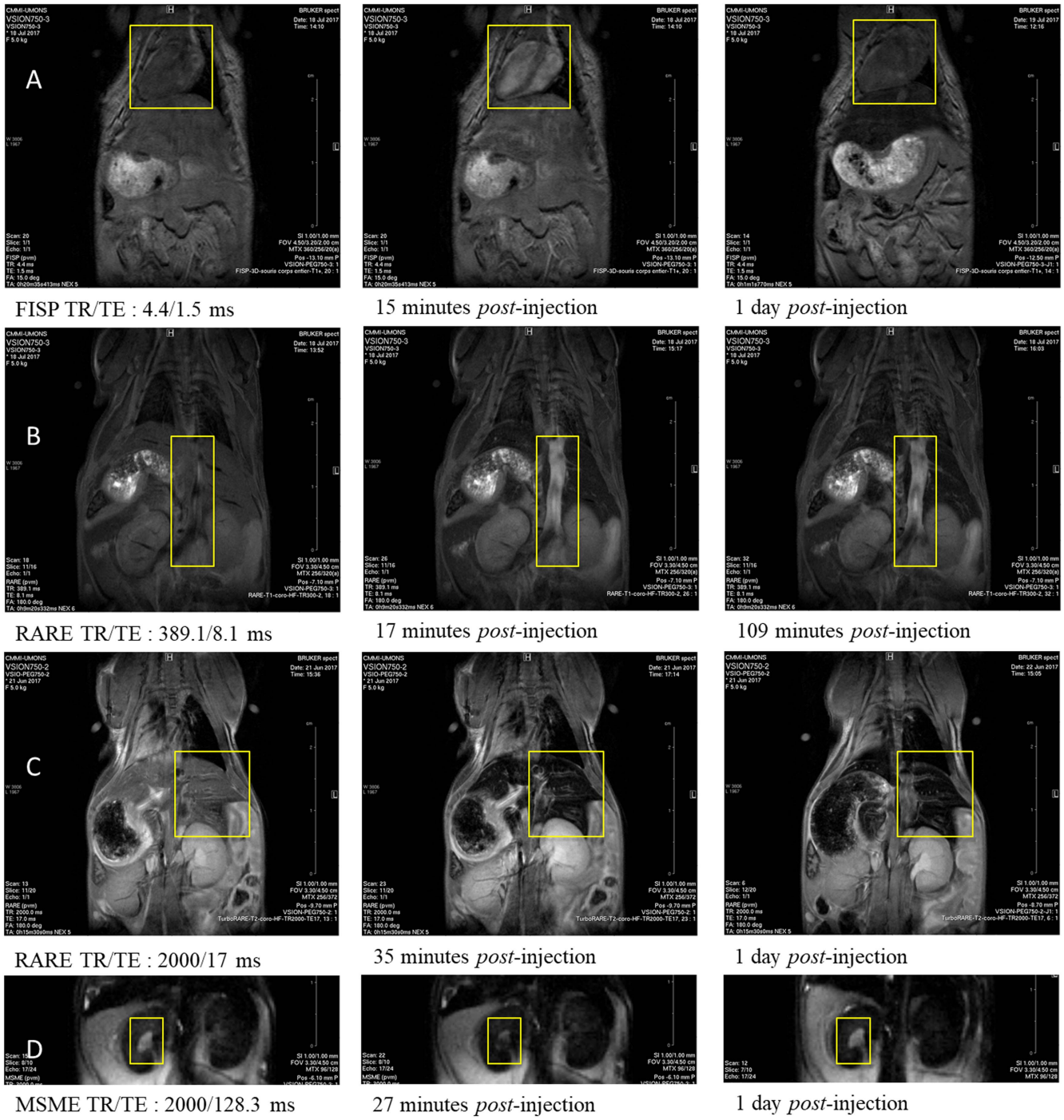

Figure 8. Illustration of *in vivo* MRI data collected on mice treated with PEG750-VSION at a dose of 45 μmol Fe kg^{-1}. (Row A) Positive signal enhancement in T_1-weighted FISP imaging before, 15 min after and one day after injection. The yellow square indicates the heart chamber in which signal intensity measurement was performed. (Row B) Positive signal enhancement in T_1-weighted RARE imaging before, 17 min after and 109 min after injection. The yellow square indicates the vena cava. (Row C) Negative signal enhancement in T_2-weighted RARE imaging before, 35 min after and one day after injection. The yellow square indicates the liver in which signal intensity measurement was performed. (Row D) Negative signal enhancement in T_2-weighted MSME imaging (17th echo (128 ms)) before, 15 min after and one day after injection. The yellow square indicates renal pelvis.

renal pelvis (figure 9(C)). The T_2 decrease, expressed as a percentage referring to the pre-injection value, reached a value ranging between 30 and 40% at 27 min post-injection. No significant difference could be seen between the two types of VSION, which showed a tendency to less markedly decreased renal pelvis T_2 with time. These results suggested that kidneys can filtrate a portion of injected VSION at early post-injection timepoints. Renal elimination of VSION is thus a mechanism to consider, together with uptake by organs of the mononuclear phagocytic system [56, 57].

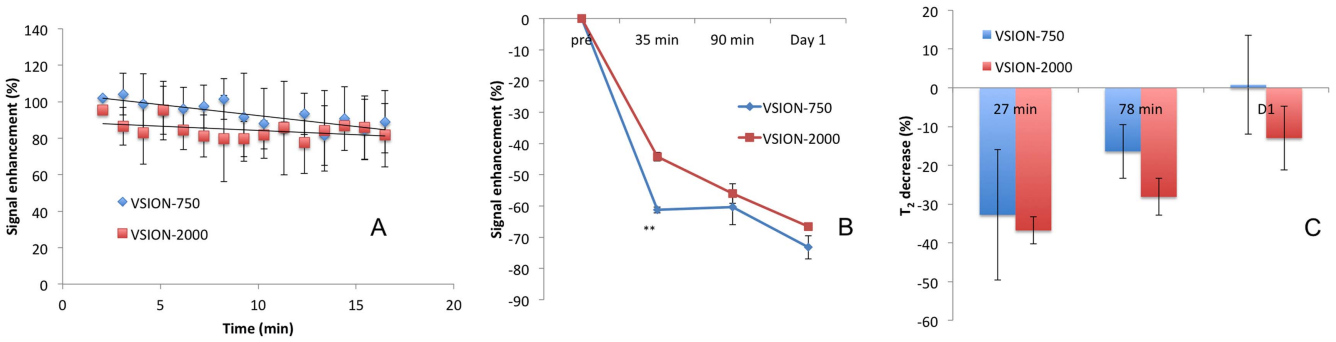

Figure 9. (A) Blood signal decrease slope from 1 min to 16 min after injection of VSION-750 or VSION-2000 (n = 3, measurement performed in main visible heart ventricle). (B) Liver negative signal enhancement in RARE imaging after injection of VSION-750 (n = 3) and VSION-2000 (n = 3 except for day 1, where n = 2) (**: $p < 0.01$). (C) Percentage of T_2 decrease measured on MSME MR images in renal pelvis at different times after injection of VSION-750 (n = 3) and VSION-2000 (n = 3 except for day 1, where n = 2).

Conclusions and outlook

In this study, the preparation of stable PEGylated VSION was demonstrated. After the development of a standard protocol allowing the synthesis of monodisperse hydrophobic 3.5 nm nanoparticles by hot injection, the as-obtained nano-objects were transferred in aqueous medium by means of a ligand exchange protocol involving the use of PEGylated bisphosphonate derivatives. Among other things, it appeared that a chain length of 17 monomer units is required in order to transfer and stabilise nanoparticles of this size and composition in aqueous media. The as-obtained suspension can be stored for three months in water or saline without any changes in their relaxivities, demonstrating their stability.

Even if 1.5 T and 3 T magnets are currently the standard in most clinics, it is probable that more performant high field (> 3 T) apparatus will appear in the near future. Interestingly, the present work demonstrates the possibility of using such platforms for T_1 high field MRA. Both presented systems showed long circulation times (> 1 h), along with hepatic and renal elimination. A slower blood elimination has been highlighted for PEG2000-VSION when compared to PEG750-VSION. Further studies involving a complementary imaging modality as well as *in vitro* experiments will start soon in order to confirm this behaviour and highlight its origin.

Acknowledgements

The authors thank the Center for Microscopy and Molecular Imaging (CMMI, supported by the European Regional Development Fund and the Walloon Region). This work was supported by the *Fond National de la Recherche Scientifique* (FNRS), UIAP VII, ARC Programs of the French Community of Belgium, COST actions and the Walloon region (Gadolymph and Holocancer programs). The authors also would like to acknowledge Emeric Carlier and Louis Van Renterghem for their contribution, as well as Das-Nano (Spain) for providing the first nanoparticles which allowed us to initiate the present study.

Conflict of interest

The authors declare that they have no conflict of interest.

ORCID iDs

T Vangijzegem https://orcid.org/0000-0001-5695-9307
S Laurent https://orcid.org/0000-0002-2589-3250

References

[1] Liang Z-P and Lauterbur P C 2000 *Principles of Magnetic Resonance Imaging: A Signal Processing Perspective* (New York: Wiley)
[2] Merbach A, Helm L and Tóth É 2013 *The Chemistry of Contrast Agents in Medical Magnetic Resonance Imaging* (New York: Wiley)
[3] Caravan P, Ellison J J, McMurry T J and Lauffer R B 1999 Gadolinium(III) chelates as MRI contrast agents: structure, dynamics, and applications *Chem. Rev.* **99** 2293–352
[4] Aimé S and Caravan P 2009 Biodistribution of gadolinium-based contrast agents, including gadolinium deposition *J. Magn. Reson. Imaging* **30** 1259–67
[5] Kiessling F *et al* 2006 Synthesis and characterization of HE-24.8: a polymeric contrast agent for magnetic resonance angiography *Bioconjugate Chem.* **17** 42–51
[6] Zhou Z, Huang D, Bao J, Chen Q, Liu G, Chen Z, Chen X and Gao J 2012 A synergistically enhanced T_1-T_2 dual-modal contrast agent *Adv. Mater.* **24** 6223–8
[7] Rogosnitzky M and Branch S 2016 Gadolinium-based contrast agent toxicity: a review of known and proposed mechanisms *Bio Met.* **29** 365–76
[8] Ramalho X J, Semelka X R C, Ramalho X M, Nunes X R H, Alobaidy X M and Castillo X M 2016 Gadolinium-based contrast agent accumulation and toxicity: an update *Am. Soc. Neuroradiol.* **37** 1192–8
[9] Robert P, Violas X, Grand S, Lehericy S, Idée J M, Ballet S and Corot C 2016 Linear gadolinium-based contrast agents are associated with brain gadolinium retention in healthy rats *Invest. Radiol.* **51** 73–82
[10] Gale E M, Atanasova I P, Blasi F, Ay I and Caravan P 2015 A manganese alternative to gadolinium for MRI contrast *J. Am. Chem. Soc.* **137** 15548–57

[11] Richard S *et al* 2016 USPIO size control through microwave nonaqueous sol-gel method for neoangiogenesis T_2 MRI contrast agent *Nanomedicine* **11** 2769–79

[12] Kim B H *et al* 2011 Large-scale synthesis of uniform and extremely small-sized iron oxide nanoparticles for high-resolution T_1 magnetic resonance imaging contrast agents *J. Am. Chem. Soc.* **133** 12624–31

[13] Estelrich J, Sánchez-Martín M J and Busquets M A 2015 Nanoparticles in magnetic resonance imaging: from simple to dual contrast agents *Int. J. Nanomedicine* **10** 1727–41

[14] Yuan-Peng R, Liang B, Hu F, Xu J, Peng Y, Yin P, Duan Y, Zhang C and Gu H 2016 Ultra-large-scale production of ultrasmall superparamagnetic iron oxide nanoparticles for T_1-weighted MRI *R. Soc. Chem.* **6** 22575–85

[15] Zhou Z, Wang L, Chi X, Bao J, Yang L, Zhao W, Chen Z, Wang X, Chen X and Gao J 2013 Engineered iron-oxide-based nanoparticles as enhanced T_1 contrast agents for efficient tumor imaging *ACS Nano* **7** 3287–96

[16] Taboada E, Rodríguez E, Roig A, Oró J, Roch A and Muller R N 2007 Relaxometric and magnetic characterization of ultrasmall iron oxide nanoparticles with high magnetization. Evaluation as potential T_1 magnetic resonance imaging contrast agents for molecular imaging *Langmuir* **23** 4583–8

[17] Neuwelt E A, Hamilton B E, Varallyay C G, Rooney W R, Edelman R D, Jacobs P M and Watnick S G 2009 Ultrasmall superparamagnetic iron oxides (USPIOs): a future alternative magnetic resonance (MR) contrast agent for patients at risk for nephrogenic systemic fibrosis (NSF)? *Kidney Int.* **75** 465–74

[18] Laurent S, Forge D, Port M, Roch A, Robic C, Vander Elst L and Muller R N 2008 Magnetic iron oxide nanoparticles: synthesis, stabilization, vectorization, physicochemical characterizations and biological applications *Chem. Rev.* **108** 2064–110

[19] Hyeon T, Lee S S, Park J, Chung Y and Na H B 2001 Synthesis of highly crystalline and monodisperse maghemite nanoystallites without a size-selection process *J. Am. Chem. Soc.* **123** 12789–801

[20] Park J, An K, Hwang Y, Park J, Noh H, Kim J, Park J, Hwang N and Hyeon T 2004 Ultra-large-scale syntheses of monodisperse nanocrystals *Nat. Mater.* **3** 891–5

[21] Smolensky E D, Park H Y E, Berquó T S and Pierre V C 2011 Surface functionalization of magnetic iron oxide nanoparticles for MRI applications—effect of anchoring group and ligand exchange protocol *Contrast Media Mol. Imaging* **6** 189–99

[22] Wu L, Mendoza-garcia A, Li Q and Sun S 2016 Organic phase syntheses of magnetic nanoparticles and their applications *Chem. Rev.* **116** 10473–512

[23] Dixit S and Jeevanandam P 2009 Synthesis of iron oxide nanoparticles by thermal decomposition approach *Adv. Mater. Res.* **67** 221–6

[24] Hufschmid R, Arami H, Ferguson R M, Gonzales M, Teeman E, Brush L N, Browning N D and Krishnan K M 2015 Synthesis of phase-pure and monodisperse iron oxide nanoparticles by thermal decomposition *Nanoscale* **7** 11142–54

[25] Chen Z 2012 Size and shape controllable synthesis of monodisperse iron oxide nanoparticles by thermal decomposition of iron oleate complex *Synth. React. Inorg. Met. Org. Nano-Met. Chem.* **42** 1040–6

[26] Matsumoto Y and Jasanoff A 2008 T2 relaxation induced by clusters of superparamagnetic nanoparticles: Monte Carlo simulations *Magn. Reson. Imaging* **26** 994–8

[27] Roca A G, Veintemillas-Verdaguer S, Port M, Robic C, Serna C J and Morales M P 2009 Effect of nanoparticle and aggregate size on the relaxometric properties of MR contrast agents based on high quality magnetite nanoparticles *J. Phys. Chem.* B **113** 7033–9

[28] Wagner M, Wagner S, Schnorr J, Schellenberger E, Kivelitz D, Krug L, Dewey M, Laule M, Hamm B and Taupitz M 2011 Coronary MR angiography using citrate-coated very small superparamagnetic iron oxide particles as blood-pool contrast agent: initial experience in humans *J. Magn. Reson. Imaging* **34** 816–23

[29] Roch A, Gossuin Y, Muller R N and Gillis P 2005 Superparamagnetic colloid suspensions: Water magnetic relaxation and clustering *J. Magn. Magn. Mater.* **293** 532–9

[30] Roch A, Muller R N and Gillis P 1999 Theory of proton relaxation induced by superparamagnetic particles *J. Chem. Phys.* **110** 5403–11

[31] Boutry S, Forge D, Burtea C, Mahieu I, Murariu O, Laurent S, Vander Elst L and Muller R N 2009 How to quantify iron in an aqueous or biological matrix: a technical note *Contrast Media Mol. Imaging* **4** 299–304

[32] Van Embden J, Chesman A S R and Jasieniak J J 2015 The heat-up synthesis of colloidal nanocrystals *Chem Mater.* **27** 1–47

[33] Thanh N T K, Maclean N and Mahiddine S 2014 Mechanisms of nucleation and growth of nanoparticles in solution *Chem. Rev.* **114** 7610–30

[34] Kwon S G, Piao Y, Park J, Angappane S, Jo Y, Hwang N, Park J and Hyeon T 2007 Kinetics of monodisperse iron oxide nanocrystal formation by 'heating-up' process *J. Am. Chem. Soc.* **129** 12571–84

[35] Salas G, Casado C, Teran F J, Miranda R, Serna C J and Morales M P 2012 Controlled synthesis of uniform magnetite nanocrystals with high-quality properties for biomedical applications *J. Mater. Chem.* **22** 21065–75

[36] Guardia P, Pérez-Juste J, Labarta A, Batlle X and Liz-Marzán L M 2010 Heating rate influence on the synthesis of iron oxide nanoparticles: the case of decanoic acid *Chem. Commun.* **46** 6108–10

[37] Wei Y, Zhang C, Chang Q, Wang X and Niu L 2017 Synthesis of monodisperse iron oxide nanoparticles: effect of temperature, time, solvent and surfactant *Inorg. Nano-Met. Chem.* **47** 1–5

[38] Belaïd S, Laurent S, Vermeech M, Vander Elst L, Perez-Morga D and Muller R N 2013 A new approach to follow the formation of iron oxide nanoparticles synthesized by thermal decomposition *Nanotechnology* **24** 1–8

[39] Baaziz W, Pichon B P, Fleutot S, Liu Y, Lefevre C, Greneche J, Toumi M, Mhiri T and Begin-Colin S 2014 Magnetic iron oxide nanoparticles: reproducible tuning of the size and nanosized-dependent composition, defects, and spin canting *J. Phys. Chem.* **118** 3795–810

[40] De la Fuente J M and Grazu V 2012 *Nanobiotechnology: Inorganic Nanoparticles vs Organic Nanoparticles* (Amsterdam: Elsevier)

[41] Mutin P H, Guerrero G and Vioux A 2005 Hybrid materials from organophosphorus coupling molecules *J. Mater. Chem.* **15** 3761–8

[42] Gao W, Dickinson L, Grozinger C, Morin F G and Reven L 1996 Self-assembled monolayers of alkylphosphonic acids on metal oxides *Langmuir* **12** 6429–35

[43] Wan J, Yuan R, Zhang C, Wu N, Yan F and Yu S 2016 Stable and biocompatible colloidal dispersions of superparamagnetic iron oxide nanoparticles with minimum aggregation for biomedical applications *J. Phys. Chem.* **120** 23799–806

[44] Bouzide A, LeBerre N and Sauvé G 2001 Silver(I) oxide-mediated facile and practical sulfonylation of alcohols *Tetrahedron Lett.* **42** 8781–3

[45] Bouzide A and Sauvé G 2002 Silver(I) oxide mediated highly selective monotosylation of symmetrical diols. Application

to the synthesis of polysubstituted cyclic ethers *Org. Lett.* **4** 2329–32

[46] Thompson M S, Vadala T P, Vadala M L, Lin Y and Riffle J S 2008 Synthesis and applications of heterobifunctional poly (ethylene oxide) oligomers *Polymer* **49** 345–73

[47] Blazewska K 2013 McKenna reaction—which oxygen attacks bromotrimethylsilane? *J. Org. Chem.* **79** 408–12

[48] Yang K, Peng H, Wen Y and Li N 2010 Re-examination of characteristic FTIR spectrum of secondary layer in bilayer oleic acid-coated Fe_3O_4 nanoparticles *Appl. Surf. Sci.* **256** 3093–7

[49] Zhang L, He R and Gu H C 2006 Oleic acid coating on the monodisperse magnetite nanoparticles *Appl. Surf. Sci.* **253** 2611–7

[50] Hannecart A *et al* 2015 Nano-thermometer with thermo-sensitive polymer grafted USPIOs behaving as positive contrast agents in low-field MRI *Nanoscale* **4** 1166–9

[51] Guénin E, Lalatonne Y, Bolley J, Milosevic I, Platas-Iglesias C and Motte L 2014 Catechol versus bisphosphonate ligand exchange at the surface of iron oxide nanoparticles: towards multi-functionalization *J. Nanoparticle Res.* **16** 2596

[52] Dedourkova T, Kaman O, Veverka P, Koktan J, Veverka M, Kulickova J, Jirak Z and Herynek V 2015 Clusters of magnetic nanoparticles as contrast agents for MRI: effect of aggregation on transverse relaxivity *IEEE Trans. Magn.* **51** 1–3

[53] Gossuin Y, Gillis P, Hocq A, Vuong Q L and Roch A 2009 Magnetic resonance relaxation properties of superparamagnetic particles *Nanomedicine and Nanobiotechnology* **1** 299–310

[54] Tromsdorf U I, Bruns O T, Salmen S C, Beisiegel U and Weller H 2009 A highly effective, nontoxic T_1 MR contrast agent based on ultrasmall PEGylated iron oxide nanoparticles *Nano Lett.* **9** 4434–40

[55] Owens D E and Peppas N A 2006 Opsonization, biodistribution, and pharmacokinetics of polymeric nanoparticles *Int. J. Pharm.* **307** 93–102

[56] Alexis F, Pridgen E, Molnar L K and Farokhzad O C 2008 Factors affecting the clearance and biodistribution of polymeric nanoparticles *Mol. Pharm.* **5** 505–15

[57] Longmire M, Choyke P L and Kobayashi H 2008 Clearance properties of nano-sized particles and molecules as imaging agents: consideration and caveats *Nanomedicine* **3** 703–17